J. Fluid Mech. (1984), *vol.* 147, *pp.* 105–131
Printed in Great Britain

Turbulent buoyant convection from a source in a confined two-layered region

By MIKIO KUMAGAI†
Research School of Earth Sciences, The Australian National University,
G.P.O. Box 4, Canberra, A.C.T. 2601, Australia

(Received 2 September 1983 and in revised form 18 April 1984)

We consider the time evolution of a layer of fresh water placed on top of a layer of salt water in a laboratory tank when denser salt water is supplied to a nozzle at the free surface. The inflow is carried out slowly so as to form a pure plume, which at first does not penetrate through the interface. The two basic processes that govern the time evolution of the initially fresh-water layer are the filling-box process (Baines & Turner 1969) and the entrainment through the end of the plume which impinges upon the density interface. A theoretical model that takes these two processes into account is presented, with the numerical solution of the asymptotic state, valid at large times. The asymptotic solution and experiment are in good agreement; the theory describes well the vertical buoyancy profile, the change in buoyancy difference across the interface with time, and the time when the plume begins to penetrate through the interface. The entrainment rate obtained from changes in thickness of the upper layer with time can be expressed as a function of the Froude number. The functional dependence is close to Fr^3 at small values of Fr, and it approaches a finite limit as Fr increases. The buoyancy flux across the interface, which is non-dimensionalized by the rate of buoyancy input, also changes as a function of Fr, taking a maximum value of 0.168 at $Fr = 0.46$ and decreasing sharply at larger and smaller Froude numbers. These values agree well with those found from field observations and experiments on the entrainment at the boundary of convectively mixed layers. It is pointed out that some earlier results of Baines (1975) are not consistent with the model presented here.

1. Introduction

Penetrative convection is defined as the process whereby convective motions arising in an unstable region penetrate into an adjacent stable layer (Turner 1973). Important examples of this process include the development of the turbulent atmospheric boundary layer during early-morning heating in the absence of strong wind, and the deepening of the thermocline in the ocean and in lakes caused by surface cooling. Since the concentrations of matter, for example pollutants emitted from smoke stacks into the atmospheric boundary layer and nutrients in the upper oceanic mixed layer, largely depend on the thickness of the layers, it is of particular importance to elucidate the mechanisms that control the thickness. It is known that the mixed-layer thickness depends on the concentrations of variables within, and the fluxes of variables across, the boundary layer. Many field observations on the atmospheric boundary layer have shown that heat transfer is conducted by way of

† Permanent address: Department of Chemical Engineering, The University of Tokyo, Hongo 7-3-1, Bunkyo-ku, Tokyo 113, Japan.

rising plumes or thermals originating near the surface shear layer and the downdraught in the gap between the thermals (e.g. Warner & Telford 1963, 1967; Kaimal *et al.* 1976). These convective cells have been clearly visualized by radar (Hardy & Ottersten 1969; Konrad 1970; Arnold *et al.* 1975), showing a dome-like depression at the interface produced by the impingement by the thermal, and Arnold *et al.* concluded from their data that most of the entrainment from the inversion takes place along the top of the dome. Laboratory experiments on penetrative convection by Deardorff, Willis & Lilly (1969), Deardorff, Willis & Stockton (1980) and Kantha (1980) have also shown that convective elements such as buoyant plumes or thermals play an important role in redistributing properties within the mixed layer and in entraining fluid from an adjacent stable layer.

We have investigated these two processes of mixing and entrainment using a salt plume discharged from a nozzle at the middle of the free surface of a water column that is initially stratified in two layers. Experiments on penetrative convection reported so far have all been carried out using a uniform distribution of buoyancy flux. The use of an isolated source allows us to understand the dynamics of the plume and environment explicitly. By this means the observed buoyancy flux across a density interface will be given a clear physical explanation, and the relation to the entrainment experiments using oscillating grids by Turner (1968) and others will be made clear.

A theoretical model to be developed in this paper to describe the motion of a plume in a confined two-layered region draws heavily on the filling-box model of Baines & Turner (1968, hereinafter referred to as BT). A good example of this process may be found in a room that is heated by a stove (with negligible radiation) at the centre of the floor. It is a common experience that it takes a long time until the air around people in the room becomes warm, although the air near the ceiling is heated quickly. The essential feature of this process is that the air heated by the stove is lifted towards the ceiling by buoyancy, spreads out along the ceiling and fills the room gradually from above. An important consequence is that a stable temperature gradient is produced in spite of the fact that the room is heated from below. This process, first extensively investigated by BT and now known as a 'filling-box' process (Turner 1973), is encountered in many different situations, and has recently been subjected to extensive investigation; for example, LNG tank stratification consequent on filling procedures (Smith & Germeles 1974) and stratification in a river-dominated lake (Killworth & Carmack 1979).

This filling-box model was successfully applied to the investigation of the convective boundary layer. When the lower part of the atmosphere is heated from the ground, the heat flux is always directed upwards, but often neutral or slightly stable buoyancy gradients are observed (Warner & Telford 1967; Kaimal *et al.* 1976; Moores *et al.* 1979). This cannot be predicted by simple mixing-length theory, which concludes that the flux must be zero or directed down the gradient of buoyancy. This phenomenon of 'transport against the gradient' was given a clear physical explanation in terms of the filling-box model by BT.

The assumption of a fixed rigid boundary, however, makes the BT model a little unrealistic when applied to the atmospheric boundary layer and the upper-ocean mixed layer. Often the capping inversion (or the thermocline) is rising (or deepening) with time by entraining the fluid of an adjacent stable layer. In this paper an extension of the BT model is presented which includes such a moving density interface and entrainment across it.

This extension requires a few problems to be solved. First, the rate of entrainment

at a density interface caused by the impingement of a plume must be made clear. Various ways to produce turbulence such as oscillating grids, a surface stress, surface jets and bottom currents, have been used to investigate the entrainment at density interfaces (see reviews by Turner 1973, 1981; Sherman, Imberger & Corcos 1978), but there are very few reports on the entrainment by plume impingement. The second problem arises from the advancement of the interface into an adjacent layer owing to entrainment, for a new time-dependency is introduced by an increase in depth of the region concerned as well as the time-dependency caused by the accumulation of buoyancy. Killworth & Turner (1982) have investigated plumes with time-varying buoyancy released from a point source in a confined region, and Worster & Huppert (1983) have presented an approximate analytic expression which can describe well the time-dependent density profile in a filling box before the asymptotic state is established. These two investigations have dealt with the region of constant depth, whereas we have to consider the effects of depth that increases with time.

A similar problem to ours has been investigated by Baines (1975). One of his main results is a linear relation between the dimensionless buoyancy flux $F^{*\prime}$ and the Froude number Fr, which extends up to $F^{*\prime} = 1.2$ at $Fr = 1.1$. However, a simple energy argument indicates that $F^{*\prime}$ cannot exceed unity, the so-called Ball limit (Ball 1960), and the theory presented here will show that there is a more strict restriction that $F^{*\prime} < 0.41$. About half of the data by Baines exceed this theoretical upper limit. Thus his results need reexamination.

The theoretical model is presented in §2. This will cover the whole process up to the penetration of a plume which occurs when the density difference between the two layers vanishes. The theory of the asymptotic state is also presented in this section with some numerical solutions. A brief description of the laboratory experiments is given in §3, and the results are presented and some are compared with the theory in §4. A detailed discussion on the entrainment across the density interface is made in §5. First, we make comments on Baines (1975) in §5.1 to show some problems in his results, and then compare our results with other experiments on entrainment particularly by Turner (1968) and Linden (1973) in §5.2. Finally, in §5.3 we discuss the relevance of this work to the laboratory experiments on penetrative convection and the field observations of the entrainment at the boundary of convectively mixed layers in the atmosphere and a lake.

2. Theoretical model

Consider the discharge of concentrated salt solution at a steady rate from a small nozzle at the middle of the free surface of a water column that is initially stratified in two layers. The volume flow rate is small enough to yield a pure buoyant plume which does not penetrate the interface. The evolution of the system observed is shown in figure 1.

On leaving the source the dense fluid forms a linearly spreading plume by entraining the ambient fluid. The first fluid to reach the interface spreads out and produces a layer with a discontinuity or front above it, marked by dye in figure 1 (*a*). As the plume fluid successively arrives at the interface and spreads along it, the first front is pushed upwards as shown in figure 1 (*b*). When sufficient salt has accumulated to cause the difference in density between the two layers to decrease to zero, the plume begins to penetrate through the interface as shown in figure 1 (*d*). Figures 1 (*d–f*) show the three-layer structure formed thereafter and the transport of fluid marked by dye. This could be described by the BT model in principle or preferably by the numerical

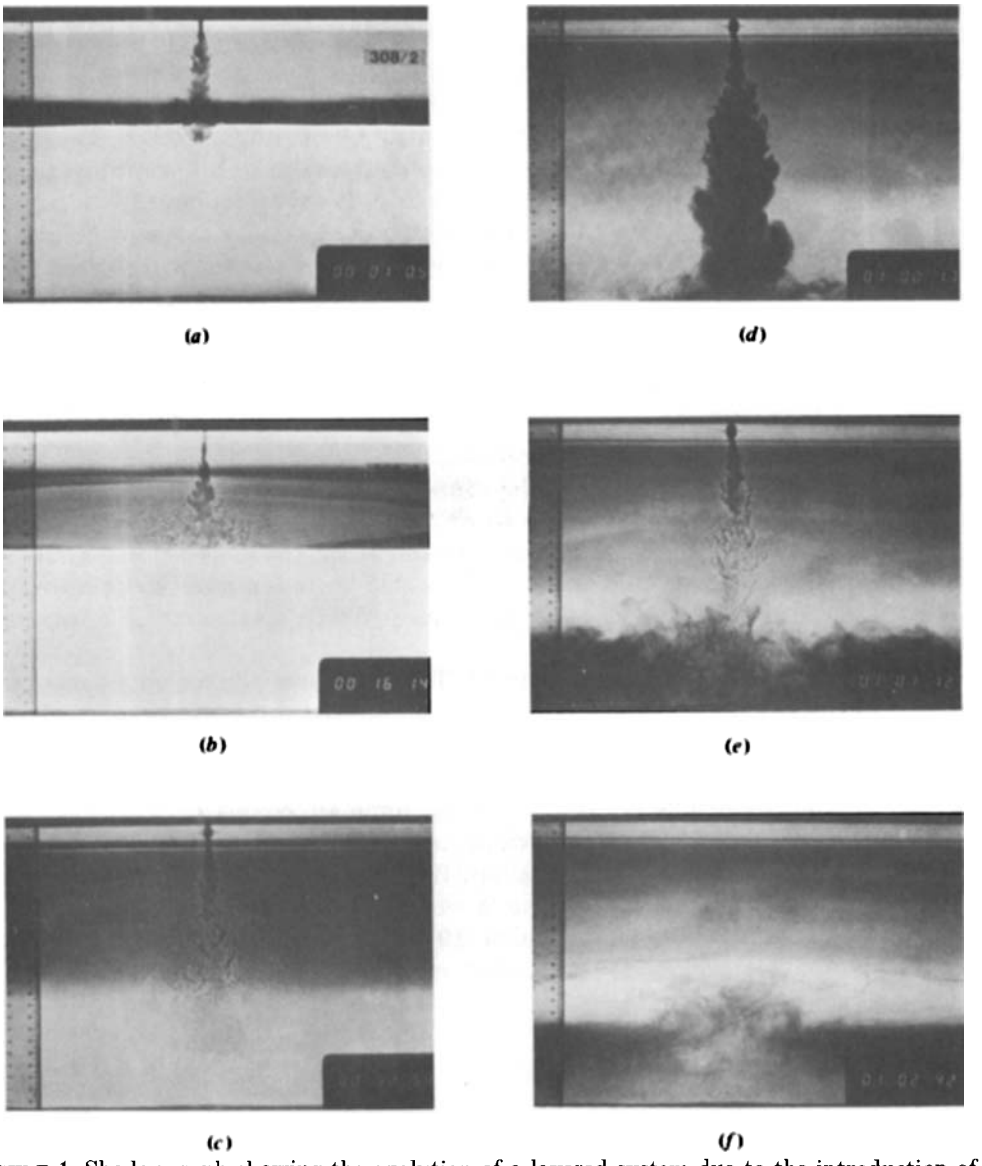

FIGURE 1. Shadowgraph showing the evolution of a layered system due to the introduction of a plume of dense salt solution of $\rho = 1.1344$ g/ml at $F = 14.1$ cm^4/s^3. Upper layer was initially fresh water 8.24 cm deep. Lower layer is salt solution of $\rho_2 = 1.0161$ g/ml. The time from the start in hours, minutes and seconds is indicated by the clock at the bottom. Depressions of the interface formed by the impingement of the plume are apparent in (*a*)–(*c*), which also show the rise of the first front. (*c*) shows a state just before the beginning of the penetration of the plume. (*d*), (*e*) and (*f*) show the spread of the plume fluid after penetration, made visible by the addition of dye. (*f*) shows the resulting three-layer structure.

model of Germeles (1975). The most significant feature of figures (*a*)–(*c*) is the deepening of the interface between the upper and lower layers. Apparently this can be attributed to the entrainment caused by the plume impingement upon the interface.

We have introduced several simplifying assumptions to model the processes described above. First, we have assumed 'top-hat' profiles for the velocity and

density distributions in a plume, following Morton (1956). This is different from the assumption of BT and Baines (1975), who have used Gaussian profiles. Though essential conclusions do not depend on the exact analytic form chosen for the profiles, it should be noted that there are differences in value of plume variables; for example, the Froude number defined by (2.7) is $2^{\frac{5}{2}}$ times larger for the Gaussian profile than for the top-hat profile. We have also introduced the usual assumptions of a Boussinesq fluid and a constant coefficient of the entrainment across the edge of a plume (Morton, Taylor & Turner 1956; BT). Manins (1979) has shown that the plume of the BT model can be considered as steady, and we assume that this is the case here.

Then, the equations of conservation of volume, momentum and buoyancy for the plume become (Turner 1973)

$$\left.\begin{aligned} \frac{\mathrm{d}}{\mathrm{d}z}(b^2w) &= 2\alpha bw, \\ \frac{\mathrm{d}}{\mathrm{d}z}(b^2w^2) &= b^2\Delta, \\ \frac{\mathrm{d}}{\mathrm{d}z}(b^2w\Delta) &= -b^2w\frac{\partial\Delta_1}{\partial z}. \end{aligned}\right\} \tag{2.1}$$

Here z denotes the depth measured downwards from the exit of the nozzle, α is the entrainment coefficient, b and w are respectively the width and velocity of the plume, and Δ and Δ_1 are the buoyancies of the plume and the upper-layer fluid, defined by

$$\Delta = \frac{g(\rho-\rho_1)}{\rho_0}, \quad \Delta_1 = \frac{g(\rho_1-\rho_0)}{\rho_0}.$$

As usual g and ρ denote respectively acceleration due to gravity and density. Subscripts 1 and 2 denote the upper- and lower-layer fluids, and ρ_0 is a reference density. Note that the buoyancy of the plume is defined relative to the ambient fluid at the same height.

There is a weak upwelling motion with velocity U in the upper layer caused by the entrainment into the plume. The conservation of volume for the total area prescribes (see figure 2)

$$R^2U = b^2w, \tag{2.2}$$

where it has been assumed that $R^2 \gg b^2$ and πR^2 is the cross-sectional area of the tank. It is also assumed that there is no mixing or diffusion in the upper-layer environment. The change in buoyancy of the environment is thus described by

$$\frac{\partial\Delta_1}{\partial t} - U\frac{\partial\Delta_1}{\partial z} = 0. \tag{2.3}$$

As the initial condition we assume a homogeneous upper layer with $\Delta_1 = 0$ and thickness H_0, and a homogeneous lower layer of buoyancy Δ_2, which remains unchanged throughout the experiment, and that the plume begins to be supplied at $t = 0$. The boundary conditions at $z = 0$ are to specify the source to be a point source supplying buoyancy only;

$$b^2w\Delta = F, \quad b^2w = b^2w^2 = 0. \tag{2.4}$$

The interface between the upper and lower layers is a moving boundary through which the entrainment of the lower-layer fluid takes place, and two relations are to be satisfied there. The first specifies the rate of descent of the interface due to the entrainment. Let H be the depth of the interface measured from the nozzle exit and

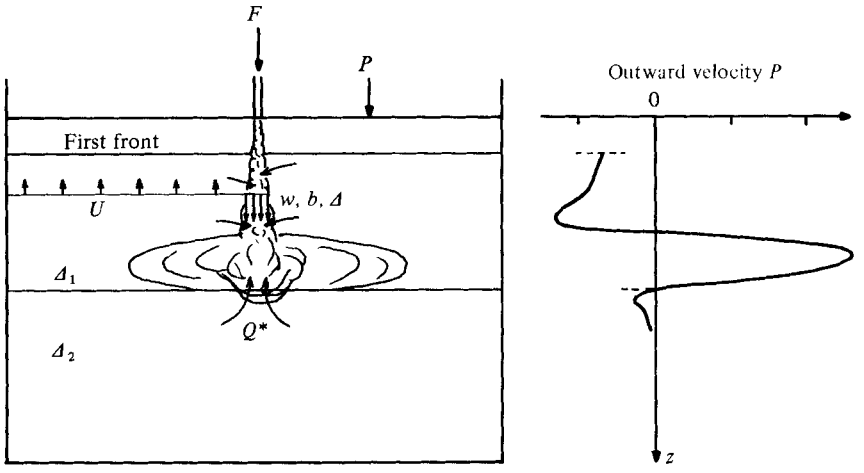

FIGURE 2. Sketch of the plume and environment, showing the motions of water and nomenclature. Entrainment occurs at the end as well as at the side boundary of the plume. The right-hand figure shows schematically the velocity profile in the ambient fluid.

Q^* be the total volume flux due to the entrainment divided by π. Then Q^* is given by

$$Q^* = R^2 \frac{\mathrm{d}H}{\mathrm{d}t}, \tag{2.5}$$

where t is the time. Baines (1975) argued that the entrainment rate must be a function of the local width, velocity and buoyancy difference, which can be combined into a single parameter, the Froude number. Linden (1973) also investigated the entrainment by vortex rings impinging upon a density interface in terms of the Froude number. We also assume that the entrainment rate is a function of the Froude number:

$$\frac{Q^*}{b_H^2 w_H} = f(Fr), \tag{2.6}$$

where

$$Fr = \frac{w_H}{(b_H \Delta_{12})^{\frac{1}{2}}}, \tag{2.7}$$

and Δ_{12} is the buoyancy difference across the interface. Note that Q^* is non-dimensionalized using the local width b_H and velocity w_H of the plume at the interface at that time. The functional form of (2.6) is left undetermined until the results of the experiments are presented. Equations (2.5) and (2.6) are combined to give the rate of increase in thickness of the upper layer as

$$\frac{\mathrm{d}H}{\mathrm{d}t} = \frac{b_H^2 w_H}{R^2} f(Fr). \tag{2.8}$$

The second condition prescribes the relation between the buoyancies of the plume and upper-layer fluid at the interface. In order to derive this relation BT have assumed that, when the plume fluid reaches the boundary, it spreads out instantaneously into a thin horizontal layer. This led to the continuity in buoyancy between them. In our experiments, however, a more complicated flow pattern was observed. The distinctive feature is the presence of circular depressions of the interface, which are continually formed and recovered; the interface is deflected downwards by the impingement of a plume at one moment and then recoils upwards owing to buoyancy.

This ejects the fluid accumulated in the depression upwards and spreads it a little distance above the interface, at about the height where the maximum of the horizontal spreading velocity appeared (figure 2). However, as Manins (1979) discussed, the details of the outflow regions are of secondary importance so long as the region occupies only a small portion of the box. Observation has shown that the thickness of the outflow region in our experiments is about 35 % of the total thickness of the upper layer. Though this is a little larger than the value of 25 % estimated for the BT model by Manins, we assume here the same flow pattern as the BT model for the sake of simplicity. The validity of this assumption is checked by experiment later. The buoyancy balance at the interface, which takes account of the entrainment of the lower-layer fluid, thus results in

$$\Delta_{1\,\mathrm{new}} = \frac{(\Delta_H + \Delta_{1H}) J_H + \Delta_2 Q^*}{J_H + Q^*}, \tag{2.9}$$

where $\Delta_{1\,\mathrm{new}}$ denotes the buoyancy of a new layer formed just underneath the upper layer at time t, and $J_H = b_H^2 w_H$. Note that the buoyancy transported by the plume is not ΔJ but $(\Delta + \Delta_1) J$. It is interesting that the interfacial phenomena described here resemble the convective cell patterns observed at the atmospheric inversion with high-power narrow-beam radars (Hardy & Ottersten 1969; Konrad 1970).

In deriving the asymptotic solution later, we shall use the total buoyancy balance in the upper layer given by

$$\frac{\partial}{\partial t} \int_0^H R^2 \Delta_1 \, \mathrm{d}z = F + \Delta_2 Q^* \tag{2.10}$$

instead of (2.9). Use has been made of the assumption that $R^2 \gg b^2$. Applying Leibniz's rule for the differentiation of integrals with variable limits to (2.10) results in

$$R^2 \int_0^H \frac{\partial \Delta_1}{\partial t} \mathrm{d}z = F + \Delta_{12} Q^*, \tag{2.11}$$

with the aid of (2.5), where Δ_{12} is the buoyancy difference across the interface defined by

$$\Delta_{12} = \Delta_2 - \Delta_1(H).$$

Equations (2.1)–(2.3) subject to (2.4), (2.8) and (2.9) or (2.11) form the theoretical model to describe the system concerned.

The equations have been non-dimensionalized, using the following scalings:

$$\left.\begin{aligned} t &= t' R^2 \alpha^{-\frac{4}{3}} F^{-\frac{1}{3}} H_0^{-\frac{2}{3}}, \\ (z, H) &= (z', H') H_0, \\ b &= b' \alpha H_0, \\ (\Delta, \Delta_1, \Delta_2) &= (\Delta', \Delta_1', \Delta_2') \alpha^{-\frac{4}{3}} F^{\frac{2}{3}} H_0^{-\frac{5}{3}}, \\ w &= w' \alpha^{-\frac{2}{3}} F^{\frac{1}{3}} H_0^{-\frac{1}{3}}, \\ U &= U' F R^{-2} \Delta_2^{-1}, \\ J &= J' \alpha^{\frac{4}{3}} F^{\frac{1}{3}} H_0^{\frac{5}{3}}, \end{aligned}\right\} \tag{2.12}$$

where primes denote non-dimensionalized variables. The dimensionless equations are

$$\frac{\mathrm{d}}{\mathrm{d}z'} (b'^2 w') = 2 b' w', \tag{2.13}$$

$$\frac{\mathrm{d}}{\mathrm{d}z'}(b'^2w'^2) = b'^2\Delta', \tag{2.14}$$

$$\frac{\mathrm{d}}{\mathrm{d}z'}(b'^2w'\Delta') = -b'^2w'\frac{\partial\Delta_1'}{\partial z'}, \tag{2.15}$$

$$U' = b'^2w', \tag{2.16}$$

$$\frac{\partial\Delta_1'}{\partial t'} - U'\frac{\partial\Delta_1'}{\partial z'} = 0, \tag{2.17}$$

and the initial and boundary conditions become

$$H' = 1, \quad \Delta_1' = 0 \quad \text{at} \quad t' = 0, \tag{2.18}$$

$$b'^2w'\Delta' = 1, \quad b'w' = b'^2w' = 0 \quad \text{at} \quad z' = 0, \tag{2.19}$$

$$\left.\begin{aligned} \frac{\mathrm{d}H'}{\mathrm{d}t'} &= b_H'^2 w_H' f(Fr), && (2.20)\\ \Delta_{1\,\mathrm{new}}' &= \frac{(\Delta_H' + \Delta_{1H}')J_H' + \Delta_2' Q^{*\prime}}{J_H' + Q^{*\prime}} && (2.21) \end{aligned}\right\} \quad \text{at} \quad z' = H',$$

where $Fr = w_H'/(\alpha b_H' \Delta_{12}')^{\frac{1}{2}}$ and $Q^{*\prime} = \mathrm{d}H'/\mathrm{d}t'$. The total buoyancy balance (2.11) is rewritten as

$$\int_0^{H'} \frac{\partial\Delta_1}{\partial t'}\mathrm{d}z' = 1 + \Delta_{12}' Q^{*\prime}. \tag{2.22}$$

These equations show that the model includes a single dimensionless parameter Δ_2', which can be externally designated. The initial depth H_0 and the buoyancy input F are already incorporated in non-dimensionalization factors. Thus the time t_p' elapsed until penetration occurs is a function of Δ_2' alone.

If the first plume fluid to reach the interface is heavier than the lower-layer fluid, the plume penetrates through the interface from the start. To avoid this, the buoyancy of the lower layer should be larger than a certain value given by

$$\Delta_2 > \frac{5F}{6\alpha}(\tfrac{9}{10}\alpha F)^{-\frac{1}{3}} H_0^{-\frac{5}{3}},$$

which in dimensionless form implies that

$$\Delta_2' > 0.8631\cdots \tag{2.23}$$

Asymptotic solution

BT have shown that as time elapses the system approaches an asymptotic state in which density is changing at the same rate at every point. This assumption needs careful examination, however, in the case of a two-layer system in which the thickness of the mixed layer and the buoyancy flux through the interface vary with time. If these changes during some timescale of the system are sufficiently slow, the state of the mixed layer will be similar to that of a single-layer filling box and will approach the asymptotic state. As shown below, this condition holds true except near the time of penetration.

An appropriate timescale for our case is the time necessary for the redistribution of fluid within the mixed layer, the so-called filling-box timescale of the order of $R^2\alpha^{-\frac{4}{3}}F^{-\frac{1}{3}}H^{\frac{2}{3}}$ given by BT. A change in H during this timescale is evaluated with the aid of (2.8) as

$$\delta H/H \sim f(Fr),$$

where we have used the approximation that $b_w^2 w_H \sim \alpha_3^{\frac{1}{3}} F^{\frac{1}{3}} H^{\frac{5}{3}}$. As shown later (figure 12), the value of $f(Fr)$ is always smaller than 0.4, and for usual values of Fr it is smaller than 0.1. It is thus found that the thickness of the mixed layer changes little during the filling-box timescale. Experimental results will show, on the other hand, that the buoyancy flux $\Delta'_{12} Q^{*\prime}$ also changes little in the course of an experiment, except at the initial transient stage and the final stage near penetration (figure 11). Thus we may assume that the two-layer system will approach the asymptotic state at large times except near the time of penetration.

Suppose that the density in the environment is changing at the same rate at all levels, and (2.22) is reduced to

$$H' \frac{\partial \Delta'_1}{\partial t'} = 1 + \Delta'_{12} Q^{*\prime} = 1 + F^{*\prime}, \quad \text{say.} \tag{2.24}$$

This equation and (2.15) and (2.17) can be combined to give a single relation which allows it to be integrated directly, yielding

$$b'^2 w' \Delta' = 1 - \frac{z'}{\beta H'}, \tag{2.25}$$

where $\beta = 1/(1+F^{*\prime})$ and the boundary condition (2.19) has been used to evaluate the constant of integration. The flux falls linearly from unity at the source, through 0 at $z' = \beta H'$, to a negative value at the interface $z' = H'$. This means that the buoyancy Δ is negative and that the plume fluid is lighter than the ambient fluid near the interface. Therefore the plume fluid tends to return and spread at its own density level. This accounts for the thicker outflowing region than that of a single-layer filling-box process.

Now it is convenient to introduce new plume variables to express deviations from the solutions for a homogeneous environment. Introduction of new variables ζ, $\tilde{J}(\zeta)$ and $\tilde{K}(\zeta)$ defined by

$$\left.\begin{aligned} \zeta &= z'/\beta H', \\ J' &= \tfrac{6}{5} (\tfrac{9}{10})^{\frac{1}{3}} z'^{\frac{5}{3}} \tilde{J}(\zeta), \\ K' &= b'w' = (\tfrac{9}{10})^{\frac{1}{3}} z'^{\frac{2}{3}} \tilde{K}(\zeta) \end{aligned}\right\} \tag{2.26}$$

reduces (2.13) and (2.14) to

$$\zeta \frac{\mathrm{d}\tilde{J}}{\mathrm{d}\zeta} = \tfrac{5}{3}(\tilde{K} - \tilde{J}), \quad \zeta \frac{\mathrm{d}\tilde{K}^4}{\mathrm{d}\zeta} = \tfrac{8}{3}\{(1-\zeta)\tilde{J} - \tilde{K}^4\}. \tag{2.27}$$

Equation (2.25) has been used in this derivation. The boundary conditions are

$$\tilde{J} = \tilde{K} = 1 \quad \text{at} \quad \zeta = 0.$$

The deviations of the width, velocity and buoyancy of the plume denoted by $\tilde{b}$, $\tilde{w}$ and $\tilde{\Delta}$ are defined, and can be calculated from $\tilde{J}$ and $\tilde{K}$, as

$$\left.\begin{aligned} b' &= \tfrac{6}{5} z' \tilde{b}, \quad \tilde{b} = \frac{\tilde{J}(\zeta)}{\tilde{K}(\zeta)}, \\ w' &= \tfrac{5}{6} (\tfrac{9}{10})^{\frac{1}{3}} z'^{-\frac{1}{3}} \tilde{w}, \quad \tilde{w} = \frac{\tilde{K}^2(\zeta)}{\tilde{J}(\zeta)}, \\ \Delta' &= \tfrac{5}{6} (\tfrac{9}{10})^{-\frac{1}{3}} z'^{-\frac{5}{3}} \tilde{\Delta}, \quad \tilde{\Delta} = \frac{1-\zeta}{\tilde{J}(\zeta)}. \end{aligned}\right\} \tag{2.28}$$

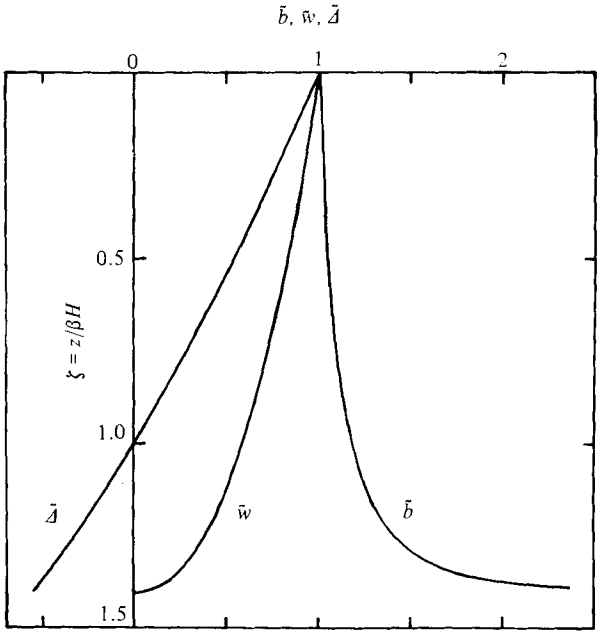

FIGURE 3. Asymptotic solutions solved numerically by the Runge–Kutta method, shown in terms of deviations from the solutions for a plume in a homogeneous environment. $\tilde{b} \to \infty$ and $\tilde{w} \to 0$ as $\zeta \to 1.41$.

The series solutions of (2.27) that satisfy the boundary conditions at $\zeta = 0$ are obtained as

$$\tilde{J}(\zeta) = 1 - 0.12821\zeta - 0.02178\zeta^2 - 0.00682\zeta^3 - 0.00270\zeta^4 - \ldots, \tag{2.29}$$

$$\tilde{K}(\zeta) = 1 - 0.20513\zeta - 0.04791\zeta^2 - 0.01909\zeta^3 - 0.00918\zeta^4 - \ldots. \tag{2.30}$$

Figure 3 shows the profiles of $\tilde{b}$, $\tilde{w}$ and $\tilde{A}$ obtained by numerical integration of (2.27) by the Runge–Kutta method with the increment of ζ of 0.005. The interface lies at $\zeta = 1/\beta$, which is larger than unity. The most significant result is that the velocity of the plume vanishes at $\zeta = 1.41$, where the width diverges to infinity. This is because the buoyancy of the plume, defined relative to the environment, becomes zero at $\zeta = 1$ and negative below this level, as shown in figure 3 or by (2.25), so that the plume is decelerated by the buoyancy force until it stops at $\zeta = 1.41$. If the interface lies above $\zeta = 1.41$ or $\beta > 1/1.41 = 0.71$, then the plume strikes the interface and is forcibly spread sideways along it before the spreading mechanism as described above comes into play. On the other hand, if the interface lies below $\zeta = 1.41$ or $\beta < 0.71$, the plume cannot reach the interface, because it spreads before reaching there. This is a curious result. The smaller β means that there is more intensive entrainment at the interface, which is realized by the impingement of a plume upon the interface; however, the assumption that $\beta < 0.71$ leads us to the contradiction that the plume cannot come into contact with the interface. It is therefore concluded that β should be always larger than 0.71 in the asymptotic state. By definition this implies that

$$F^*/F < 0.41. \tag{2.31}$$

It should be noted that this conclusion does not depend on the functional form of the entrainment rate $f(Fr)$. It will be shown later that if the functional form obtained by our experiments is assumed for $f(Fr)$ then the ratio F^*/F takes values in a much

narrower range than (2.31). Note also that (2.31) is derived under the assumption of the asymptotic state. So the observed value of β can be used to judge if the measurement was made in the asymptotic state or not.

Check of the accuracy of the series solutions (2.29) and (2.30) by comparison with the numerical solution has revealed that the series solution for $\tilde{J}(\zeta)$ (2.29) has sufficient accuracy in the whole range of ζ between 0 and 1.41, whereas (2.30) for $\tilde{K}(\zeta)$ causes serious errors at $\zeta > 1$. Therefore the use of (2.30) should be avoided, except for small values of ζ.

The time of penetration

The vertical distribution of buoyancy in the upper layer is described by

$$\frac{\partial \Delta_1'}{\partial z'} = \frac{1}{\beta H' \overline{b'^2 w'}}, \tag{2.32}$$

which is derived from (2.16), (2.17) and (2.24). Integrating (2.32) and substituting $\mathrm{d}\zeta = \mathrm{d}Z'/(\beta H')$, (2.26) and (2.29) into the resulting equation yield

$$\begin{aligned} \Delta_1' &= -\tfrac{5}{6}(\tfrac{10}{9})^{\frac{1}{3}}(\beta H')^{-\frac{5}{3}} \int_{\zeta}^{1/\beta} \frac{\mathrm{d}\zeta}{\zeta^{\frac{4}{3}} \tilde{J}(\zeta)} + C \\ &= \tfrac{5}{4}(\tfrac{10}{9})^{\frac{1}{3}}(\beta H')^{-\frac{5}{3}} \{\zeta^{-\frac{2}{3}} \delta(\zeta) - \beta^{\frac{2}{3}} \delta(1/\beta)\} + C, \end{aligned} \tag{2.33}$$

where $$\delta(\zeta) = 1 - 0.25642\zeta - 0.01911\zeta^2 - 0.00415\zeta^3 - 0.00125\zeta^4. \tag{2.34}$$

The integral constant is determined from the total buoyancy balance; that is, the integral of Δ_1' over the whole depth of the upper layer at time t' should equal the buoyancy supplied during the time interval between 0 and t'. Performing this integration results in

$$\Delta_1' = \frac{t' + \Delta_2'(H' - 1)}{H'} - \tfrac{5}{4}(\tfrac{10}{9})^{\frac{1}{3}}(\beta H')^{-\frac{5}{3}} \{\zeta^{-\frac{2}{3}} \delta(\zeta) - 3\beta^{\frac{2}{3}} \gamma(\beta)\}, \tag{2.35}$$

where $$\gamma(\beta) = 1 - 0.06411\beta^{-1} - 0.00273\beta^{-1} - 0.00042\beta^{-3} - 0.00010\beta^{-4}. \tag{2.36}$$

Putting $\zeta = 1/\beta$ in (2.35) and taking the difference from Δ_2', we have the buoyancy difference across the interface as

$$\Delta_{12}' = \frac{t_{\mathrm{p}}' - t'}{H'}, \tag{2.37}$$

where $$t_{\mathrm{p}}' = \Delta_2' - \tfrac{5}{4}(\tfrac{10}{9})^{\frac{1}{3}} H'^{-\frac{2}{3}} \beta^{-1} \{3\gamma(\beta) - \gamma(1/\beta)\}. \tag{2.38}$$

The second term of the right-hand side of (2.38) includes variables that change with time such as H' and β. However, calculation shows little change in value of this term, and so t_{p}' can be regarded as a constant depending on Δ_2' alone. The time t_{p}' thus determined expresses the time of penetration, because Δ_{12}' vanishes at $t' = t_{\mathrm{p}}'$, as shown by (2.37).

The change of β near the time of penetration can be deduced with the use of (2.25), which shows that $\Delta' < 0$ near the interface unless $\beta = 1$. In other words, the density of the plume fluid is smaller than the environment. Suppose here that $\beta < 1$ just when the buoyancy difference Δ_{12}' has vanished. The plume fluid should have a smaller density than the lower layer at this moment, so that it cannot penetrate through the interface. At the next moment the upper layer becomes heavier than the lower layer, which should result in a vigorous overturn of both layers. But this was not observed at all. Actually penetration of the plume occurred. It is therefore concluded that the

value of β should increase to unity or F^* should decrease to zero at the moment when the buoyancy difference Δ'_{12} vanishes. Note that this conclusion as well as (2.37) and (2.38) have been derived on the assumption that the asymptotic state can be assumed up to the time of penetration. This of course needs experimental examination.

3. Laboratory experiments

The experiments were carried out in a rectangular glass-walled tank 37 cm deep and 60 cm × 29.2 cm in cross-section, which was filled with two layers of fluid. The fluid in the upper layer was fresh water and the lower layer was a denser, salt solution. The temperatures of both the layers were adjusted to be the same. In order to obtain a sharp interface between the layers the fresh water was carefully added on top of the saline water through a floating sponge. The interface was then sharpened by siphoning fluid from the centre of the interface (Linden 1973). The thickness of the interface determined from the density profile was about 1 cm.

When the aspect ratio H/R was larger than unity, a vertical circulation or a general overturning of the ambient fluid could take place instead of the filling process as assumed in the theory (BT). The initial aspect ratio H_0/R was therefore set smaller than 0.5 to ensure that H/R did not exceed unity in the course of an experiment.

As soon as the siphoning finished, the nozzle, of inside diameter 5 mm, was placed at the free surface in the centre of the tank, and the salt solution, 10–13 % heavier than fresh water, was introduced through it. A flowmeter was used to control the rate of addition of salt water. The flow rate was determined from the increase in height of the free surface and the elapsed time.

In order to promote transition from laminar to turbulent flow, a piece of wire mesh was placed in the nozzle (Baines 1975), and the pipe frame to which the nozzle was fixed was weakly tapped by a soft vinyl tube fitted to a motor rotating at a rate about 1 Hz. This was weak enough to induce no motion in the water, but effectively fixed the transition point within a few millimetres from the nozzle exit. Adverse effects of tapping were checked by an experiment with no tapping (run 11, where a nozzle of inside diameter 1.8 mm was used without wire mesh). The results showed no significant difference from the other runs, though in this run the transition point moved up and down by more than 1 cm in response to external disturbances.

Vertical density profiles were measured by withdrawing 7 ml samples from 10–25 depths through a thin horizontal tube. This is 1 mm diameter and 23 cm long with eight small holes drilled into its sides and is fitted to a vertical traverse mechanism. The density was measured using a commercial densimeter (Anton Paar DMA 60/602).

A shadowgraph technique was used to follow changes in position of the first front (BT) and interface with time. To minimize errors due to reflection of light, the height of a projector was so adjusted at every measurement that the centre of the lens would be level with the first front or interface. The results of six runs where the initial and final density profiles were measured, showed that the interface positions determined from the images on the shadowgraph screen were always 2–8 mm lower than those from the density profiles, but that the lowering velocities of the interface estimated by these two methods differed by only 4 % (the shadowgraph method gave smaller values).

The advancing velocity of the first front was used to determine the entrainment coefficient α (BT). Determinations of the other variables were made as follows. Let the average of two successive observed values of $H(t)$ be $\bar{H}$ and the average time be

$\bar{t}$. The entrainment rate at $\bar{t}$, $Q^*(\bar{t})$, was estimated by differencing the successive values of $H(t)$. Since we know the time of penetration t_p, we can estimate the buoyancy difference as a function of time by (2.37) or

$$\Delta_{12}(\bar{t}) = \frac{F(t_p - \bar{t})}{R^2 \bar{H}},$$

which in turn is used to give

$$F^*(\bar{t}) = \Delta_{12}(\bar{t})\, Q^*(\bar{t})$$

and $\beta(\bar{t}) = F/(F+F^*)$. The validity of (2.37) is shown in §4. Then the velocity and width of a plume at the interface are estimated from $\bar{H}$ and $\beta(t)$ with the use of the numerically solved asymptotic-state solutions. The value of the Froude number is calculated using these results.

4. The results of experiments

Thirteen runs were carried out to cover a wide range of experimental conditions, which are shown in table 1. The buoyancy input F ranged from 7.3 to 15.6 cm^4/s^3, the buoyancy of the lower-layer fluid Δ_2 from 7.1 to 50.1 cm/s^2, and the initial thickness of the upper layer from 8.20 to 15.16 cm. As a result, the most important parameter Δ_2' was changed between 5.5 and 63.9 and the Froude number from 0.1 to 2.9.

The entrainment coefficient α was estimated from the rising velocity of the first front (BT). The value of α that emerged from the measurements on seven runs was 0.127 ± 0.025 (appropriate for the top-hat profile). The corresponding value for the Gaussian profile is 0.090, which is a little smaller than 0.100 used by BT and 0.093 by Baines (1975). In most cases the virtual source coincided with the actual nozzle exit. For the present purposes the value of $\alpha = 0.127$ found experimentally will be used throughout the data reduction.

Typical changes in the height of the interface from the bottom and the entrainment rate across the interface with time are shown in figure 4, observed in run 5. At first the interface lowers quickly with time as a result of intense entrainment. This occurs because the interface is exposed to the direct attack of a plume. When the asymptotic state is almost established, in about a filling-box timescale, the lowering of the interface slows down, and near the time of penetration the lowering velocity and therefore the entrainment rate again increase quickly. The upper layer decreases in thickness after penetration because the upper-layer fluid is transported to the bottom of the tank by the plume. The new third layer is formed on the bottom as the result of this transportation. These changes are shown in figure 1. Figure 1(*f*) is an interesting picture, for the three-layer structure looks as if it had been formed by the intrusion of the middle layer.

Before presenting results on the entrainment, we examine some assumptions made in developing the theoretical model or used to estimate some quantities such as the Froude number, the buoyancy difference, and so on. Figure 5 shows the observed profiles of vertical buoyancy distribution in the upper layer and theoretical curves given by (2.35). The datum buoyancies at $z' = 1$ were determined by extrapolating the data between $z' = 0.5$ and 0.8 to $z' = 1$. These profiles were measured at $t' = 5.2$–24.2, meaning that the asymptotic state had already been reached. Near the free surface the data lie between curves for $\beta = 1$ and $\beta = 0.75$, meaning that the profiles are certainly affected by the entrainment at the interface. With increasing

Run	Δ_{in}‖ (cm s^{-2})	Δ_2 (cm s^{-2})	F (cm^4 s^{-3})	H_0 (cm)	t_p (min)	Δ_2'	t_p'	Symbol
1	104	13.4	10.2	11.94	85	11.3	6.9	○
2	121	13.3	15.6	9.85	43	6.2	3.4	△
3	121	26.5	9.7	10.27	213	18.1	14.7	×
4	130	7.1	9.1	10.81	45	5.5	3.2	▲
5	116	43.0	10.6	6.24	184	12.1	9.4	▼
6	128	38.7	11.3	9.60	268	21.2	18.9	◑
7†	132	13.9	11.0	8.74	64	6.7	4.2	◎
8†	132	25.9	12.4	10.57	172	15.7	13.1	◩
9†	132	26.7	13.9	10.79	160	15.5	12.9	◪
10†	132	25.2	13.3	10.40	161	14.2	12.5	◐
11‡	132	50.1	10.6	8.20	350	21.3	21.1	●
12†	88.9	41.7	7.3	14.88	729	63.9	58.7	▽
13†	88.9	26.3	8.1	15.16	402	38.8	34.0	□

† F was calculated from the difference between initial and final density profiles. t_p was calculated from observed H and Δ_{12} at t by $t_p = R^2H\Delta_{12}/F+t$. Run 7 stopped at $t = 20.8$ min, run 8 at $t = 68.3$ min, run 9 at $t = 30.0$ min, run 10 at $t = 120$ min, run 12 at $t = 300$ min and run 13 at $t = 266$ min.

‡ A nozzle of inside diameter 1.8 mm was used without wire mesh or tapping of the frame.

‖ This denotes the buoyancy of the input fluid.

TABLE 1. Experimental conditions

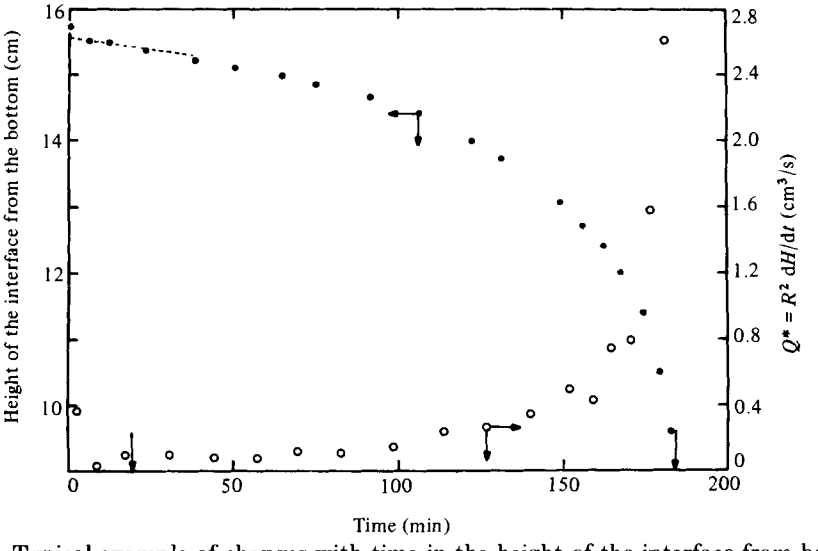

FIGURE 4. Typical example of changes with time in the height of the interface from bottom and entrainment flux across the interface (run 5). Filling-box timescale is 19.6 min, and penetration occurred at 184 min as shown by an arrow. The initial thickness estimated by extrapolation as shown by the dashed line was used instead of the observed value as a scale for non-dimensionalization (2.12). The difference of these two was 2.7% on the average.

distance from the surface, the profiles tend to become steeper than the theoretical curve. This may be caused by mixing in the outflowing region which occupies about 35% of the whole thickness of the upper layer. As a whole, however, agreement between the observation and theory is fairly good.

Figure 6 plots the dimensionless penetration time against the dimensionless

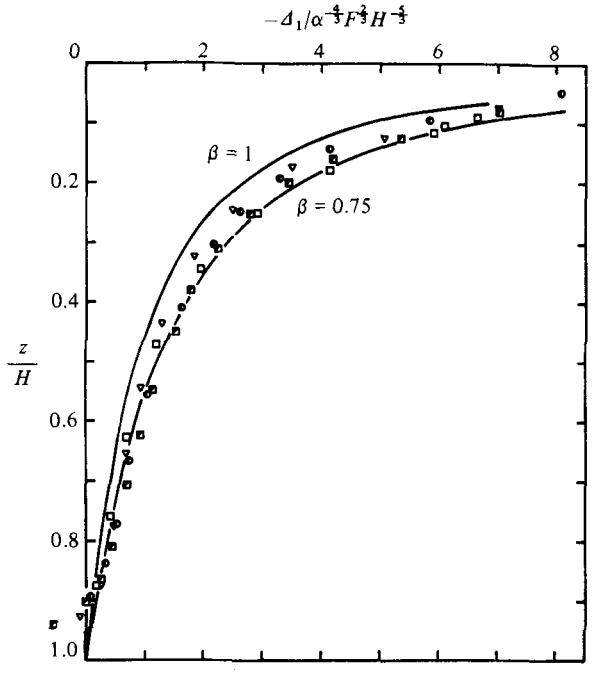

FIGURE 5. Dimensionless buoyancy distributions compared with the asymptotic state solution (2.35). Symbols as in table 1.

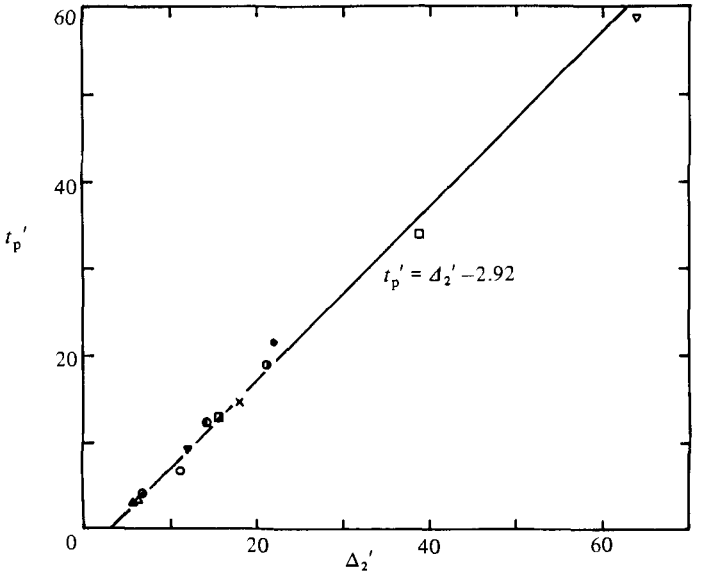

FIGURE 6. Observed time of penetration as a function of the lower layer buoyancy, except for runs 7, 8, 10, 12 and 13, for which the values of t_p are not observed times but are calculated from observed Δ_{12}', H' and t' by use of (2.37). Symbols as in table 1.

lower-layer buoyancy. There is a good linear relationship between them. The best-fit line is

$$t_p' = \Delta_2' - 2.92. \tag{4.1}$$

With $\beta = 0.85$ and $H' = 1.3$, (2.38) gives the numerical constant of 2.68. The agreement between the theory and experiments is thus very good.

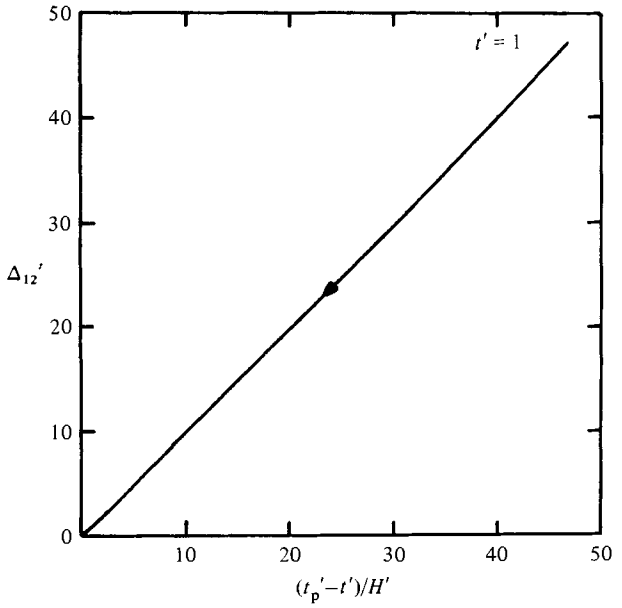

FIGURE 7. Buoyancy difference across the interface as a function of time obtained by the numerical simulation which does not assume the asymptotic state.

Note that the values of t_p for runs 7, 8, 10, 12 and 13 are not observed penetration times but times calculated from observed values of Δ_{12}', H' and t' by use of (2.37). That these data lie on the straight line given by (4.1) seems to suggest the validity of (2.37). This validity can be tested by carrying out another numerical experiment. Figure 7 shows the results of a numerical simulation which solved the complete set of equations (2.13)–(2.21) with the entrainment law given by (4.5) and without assuming the asymptotic state. The algorithm used is the same as that of Germeles (1975) with a modification to include the boundary condition (2.21). The lower-layer buoyancy Δ_2' is 50. Apparently (2.37) holds quite well from $t' = 1$ to the time of penetration. It is thus proved that (2.37) provides good estimation of the buoyancy difference across the interface throughout the course of the experiment.

Evolution of the system

Changes in the Froude number, entrainment rate, thickness of the upper layer and buoyancy flux across the interface with time are shown in figures 8–11. Only data with $t' > 2$ are plotted in figures 8–10 in order to exclude transient data taken before the asymptotic state has been established. The most significant feature is that those changes observed under a wide range of experimental conditions can be well represented by one curve, or in some cases a family of curves covering different values of the single dimensionless parameter Δ_2'.

The Froude number is at first small, its value depending on the value of t_p' or Δ_2', and increases steadily with time. In other words, the interface is becoming less stable with time. This is due to the decrease in the buoyancy difference between the upper and lower layers. Calculation shows that the magnitude of Fr is primarily dependent on Δ_{12}', which varies almost in proportion to $t_p'-t'$, so that $Fr \propto (t_p'-t')^{-\frac{1}{2}}$. This is in agreement with the tendency in figure 8.

Responding to changes in the Froude number, the entrainment rate increases steadily with time as shown in figure 9. This good correspondence suggests that the

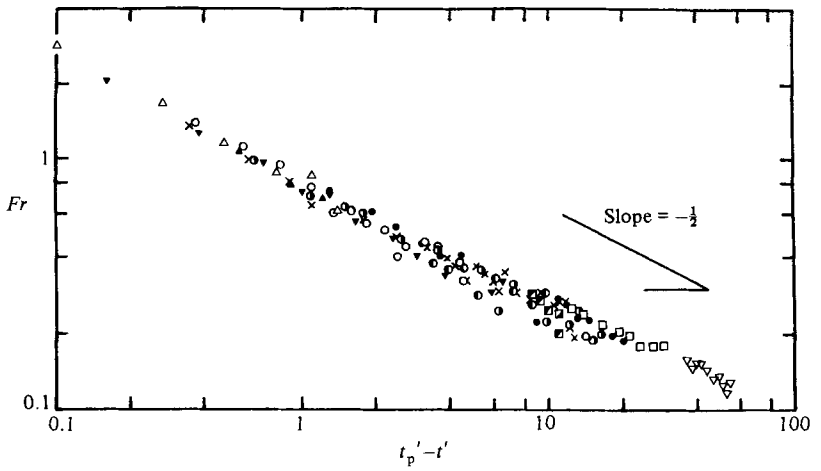

FIGURE 8. Changes in Froude number with time at $t' > 2$ when the asymptotic state is established. Symbols as in table 1.

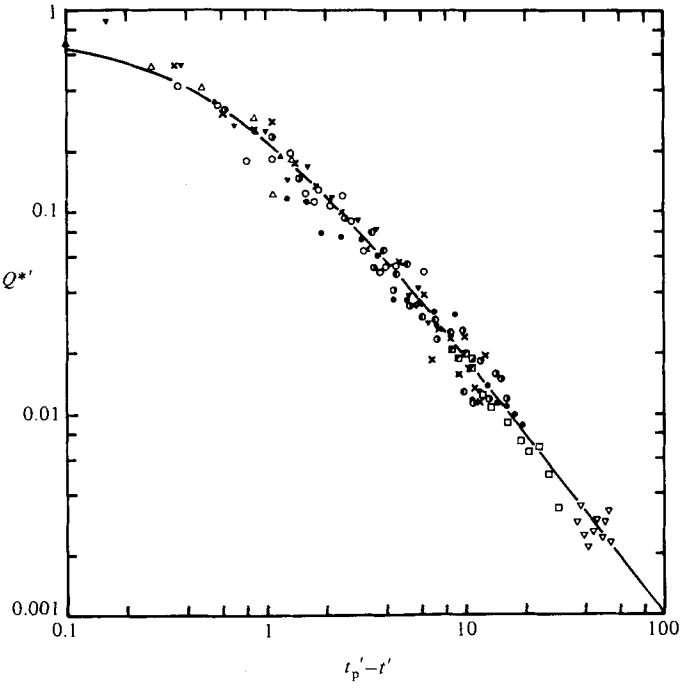

FIGURE 9. Entrainment flux as a function of time. Only data for $t' > 2$ are plotted to exclude transient data. The curve fitted to the data is $Q^{*'} = 0.41(t_p'-t'+0.6)^{-1.3}$. Symbols as in table 1.

entrainment rate is a function of the Froude number alone, as discussed by Baines (1975). A full discussion of this point is given later. The curve shown in this figure is

$$Q^{*'} = 0.41(t_p'-t'+0.6)^{-1.3}, \tag{4.2}$$

which has been chosen from several functional forms merely because it is simple and a good approximation in the sense of least-square fitting.

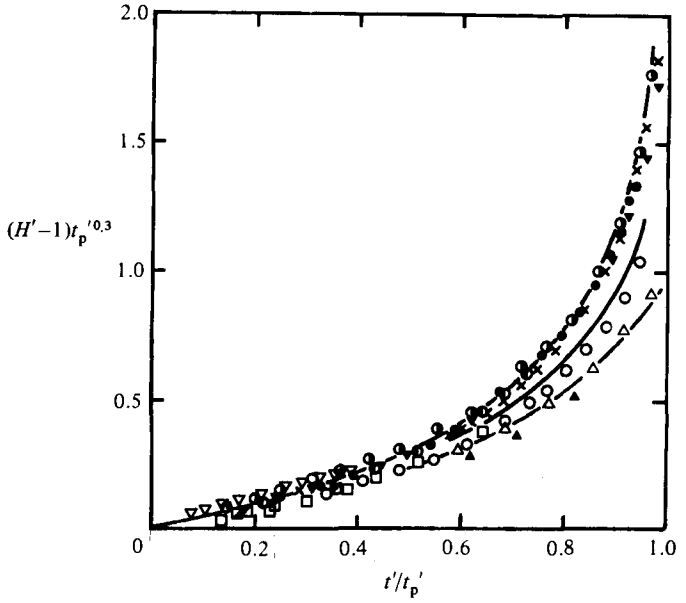

FIGURE 10. Increases in thickness of the upper layer with time at $t' > 2$. The three curves, given by (4.3), correspond from bottom to top to $t_p' = 3$, 6 and 20 respectively. Curves for runs with $t_p' > 9$ can be represented by the one for $t_p' = 20$. Symbols as in table 1.

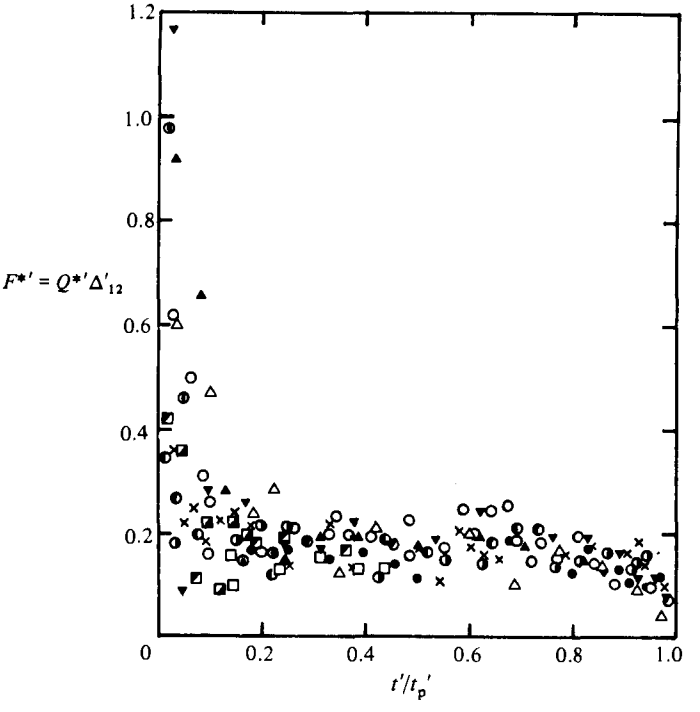

FIGURE 11. Buoyancy flux across the interface as a function of time. This includes initial transient data, unlike figures 8, 9, 10, 12 and 13. Note that $F^*/F = (1-\beta)/\beta$. Symbols as in table 1.

Since $Q^{*\prime} = \mathrm{d}H'/\mathrm{d}t'$, (4.2) can be integrated to yield H'. The result is

$$H'-1 = 1.37(t'_{\mathrm{p}}+0.6)^{-0.3}\left\{\left(1-\frac{t'}{t'_{\mathrm{p}}+0.6}\right)^{-0.3}-1\right\}. \tag{4.3}$$

Figure 10 shows the thickness of the upper layer as a function of time in a form suggested by this equation, for three different values of t'_{p}. As expected, agreement with (4.3) is very good. An interesting consequence of (4.3) is that the thickness at the time of penetration is given by

$$H' = 2.59-1.37(t'_{\mathrm{p}}+0.6)^{-0.3}, \tag{4.4}$$

which means that the maximum thickness attainable is 2.59 times of the initial thickness.

Figure 11 shows the buoyancy flux across the interface as a function of time. This figure includes transient data from initial stages, unlike the other figures. Large values observed during $t'/t'_{\mathrm{p}} = 0$–0.3 are such data. Between $t'/t'_{\mathrm{p}} = 0.3$–0.8 the data converge within a relatively narrow range around a mean of 0.18, then gradually decreasing to zero. This result is quite consistent with the theoretical predictions. The theory has required that the value of $\beta = 1/(1+F^{*\prime})$ be larger than 0.71 in the asymptotic state and increase to unity at penetration. This means that $F^{*\prime} < 0.41$ and decreases to zero as $t \to t_{\mathrm{p}}$, which agrees with the observations.

The entrainment rate

Figures 8 and 9 have suggested that the entrainment rate is a function of the Froude number. This relation is shown in figure 12. Note that the entrainment rate is normalized by the volume flux of a plume at the interface at each time. This is better than $Q^{*\prime}$ because the normalization by $b_H^2 w_H$ takes account of the change of a plume with time, whereas the non-dimensionalization factor depends only on the initial conditions.

Though scatter is large, some definite tendencies can be read from this figure. At the Froude numbers smaller than 0.3 the data can be represented fairly well by a line of slope 3, which implies the functional form of $Q^*/b_H^2 w_H \propto Fr^3$. At the larger values of Fr used the entrainment rate deviates from the Fr^3 law and approaches a constant value. This is similar to the results obtained by Turner (1968) in the measurement of entrainment caused by an oscillating grid. The data can well be represented as a whole by an empirical formula

$$\frac{Q^*}{b_H^2 w_H} = \frac{1.0Fr^3}{1+3.1Fr^2+1.8Fr^3}. \tag{4.5}$$

This reduces to $1.0Fr^3$ at $Fr \ll 1$ and approaches 0.56 as $Fr \to \infty$, though an observed maximum value was 0.32.

The buoyancy flux across the interface

The buoyancy flux at the asymptotic state is plotted in figure 13 as a function of the Froude number. An important feature is that the value of F^*/F takes a maximum at around $Fr = 0.46$ and decreases sharply at smaller and larger Froude numbers. The decrease in the buoyancy flux at the larger values of Fr may be understood by noting that large Froude numbers are realized only when the buoyancy difference is reduced to small values by the accumulation of salt. The curve in this figure was obtained using the entrainment law given by (4.5), Δ'_{12} by (2.37), H' by (4.3) and the

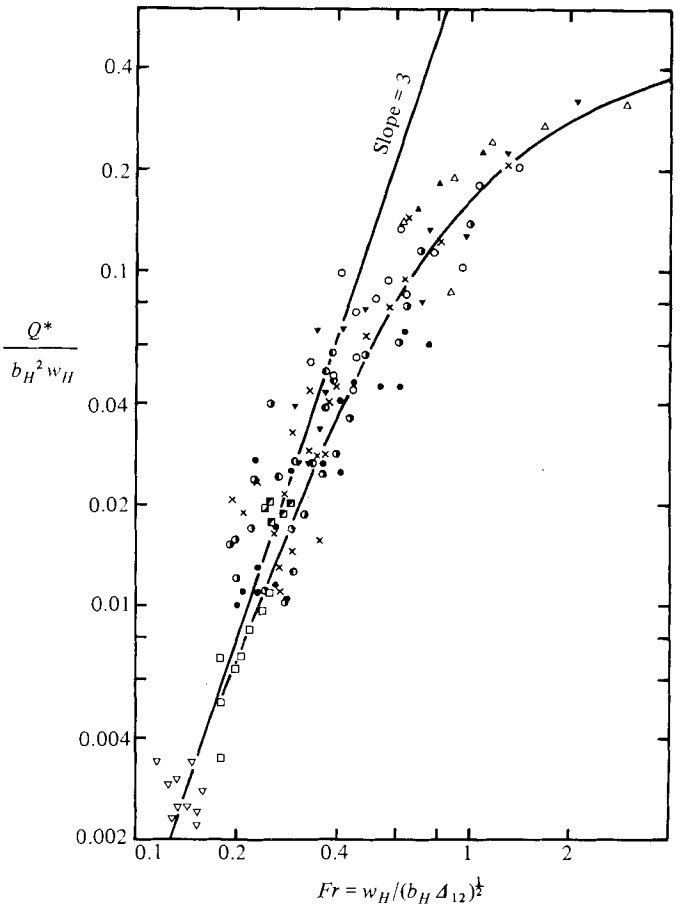

FIGURE 12. Entrainment volume flux as a function of Fr observed at $t' > 2$. The curve is given by $Q^*/b_H^2 w_H = 1.0Fr^3/(1+3.1\ Fr^2+1.8Fr^3)$. Symbols as in table 1.

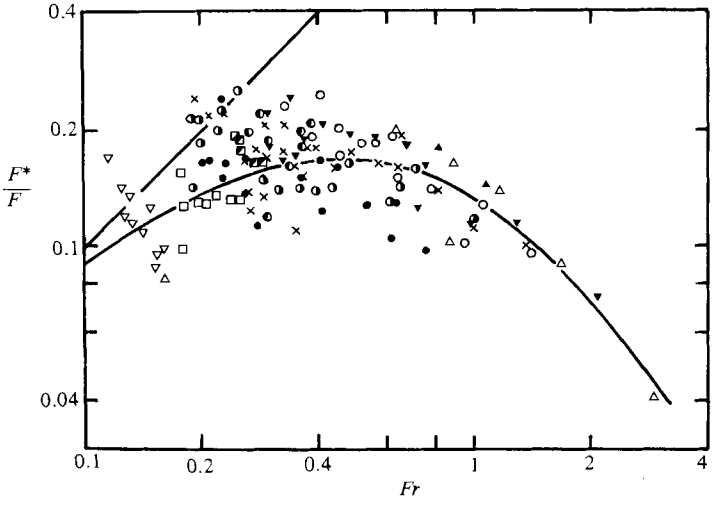

FIGURE 13. Buoyancy flux across the interface as a function of Fr observed at $t' > 2$. The curve is a theoretical prediction based on figure 12. The straight line is the result of Baines (1975). Symbols as in table 1.

numerically solved asymptotic solutions. Though the data at $Fr < 0.5$ are very scattered, agreement is fairly good. The straight line is the result of Baines (1975), and comments are given in §5.1.

5. Discussion

5.1. *Comments on Baines* (1975)

There are some differences between our results and those of Baines (1975, hereinafter referred to as B). The most obvious and serious difference emerges from comparison of the buoyancy fluxes across the interface. The conclusion of B is a linear relationship between F^*/F and Fr, partly reproduced as a straight line in figure 13. This is apparently inconsistent with our results. The data of B extend up to $F^*/F = 1.2$ at Fr = 1.1, while at this value of Fr our result is $F^*/F = 0.125$, only 10 % of the above value (figure 13). As shown in §2, the value of β should always be larger than 0.71, and the dimensionless buoyancy flux F^*/F cannot exceed 0.41 in the asymptotic state. About half of the data of B exceed this theoretical upper limit. The problem in B is also revealed by a simple energy argument, presented in §5.3, that the dimensionless buoyancy flux is equal to the ratio of the increase in potential energy due to the redistribution of the initial density profile, to the potential energy made available by buoyancy input. It is evident from this argument that F^*/F cannot be larger than unity; however, the results of B include a datum point that violates this restriction.

These differences seem to be attributed to the different definition of the buoyancy flux across the interface; B's definition is

$$F^* = \Delta_2 Q^*,$$

while ours is

$$F^* = \Delta_{12} Q^*.$$

As shown in deriving (2.11), the use of the buoyancy difference Δ_{12} is correct in general. However, if the depth of the upper layer can be assumed constant, B's definition can be a good approximation. For example, at early times of a run that starts with a large buoyancy difference or a small initial Froude number, the depth of the upper layer will remain almost unchanged and $\Delta_{12} \approx \Delta_2$. B's results for small values of Fr are thus close to ours; the volume entrainment flux Q^* increased with Fr^3, and the buoyancy flux F^* increased with Fr at small values of Fr, in good agreement with the tendencies in figures 12 and 13.

At large values of Fr, however, the constant-depth approximation can no longer hold, resulting in overestimation of the buoyancy flux. Too-large values of F^*/F in B seem to have resulted from this overestimation. The relation between Q^* and Fr is also incorrect, because Fr depends on the width and velocity of a plume at the interface, which depend on the value of F^*. Thus the results in B, which are based on the constant-depth approximation, are correct only at small values of Fr.

5.2. *Entrainment rate*

A number of laboratory experiments of two types have been performed to clarify the processes of entrainment against a density jump. In the first kind, which has been extensively investigated by Turner (1968, 1973), the turbulence is produced by stirring mechanically either in one or in both layers. He found that the ratio of entrainment velocity to stirring velocity can be expressed as functions of an overall Froude number. For density differences produced by heat alone, the functional

dependence is close to Fr^2 except at large values of Fr, where it approaches a finite limit. For experiments with a salinity difference across the interface, the mixing rate is the same as in the heat experiments at large values of Fr, but falls progressively below this as Fr is decreased, with the approximate form Fr^3. These results were confirmed by Wolanski & Brush (1975) and Hopfinger & Toly (1976). In these experiments there is no significant mean flow or shear. The second type of experiment involves shear-flow turbulence produced either by a surface stress in an annular tank (Kato & Phillips 1969; Kantha, Phillips & Azad 1977), or by way of surface jets or bottom currents (Ellison & Turner 1959; Lofquist 1960). These results are discussed in detail by Turner (1973).

Our experiments correspond to the first type with a salinity difference, since there is no significant mean flow. Interestingly the relation between the dimensionless entrainment rate and the Froude number shown in figure 12 is qualitatively in good agreement with Turner's result, in spite of the fact that the turbulence is produced in different ways. Some appropriate scaling for velocity and length could bring a good quantitative agreement.

A mechanistic explanation of the Fr^3 mixing law was proposed by Linden (1973) based on the investigation on vortex rings projected against a sharp density interface. Observation showed that the interface was deflected downwards by the ring and then recoiled to cause the fluid accumulated in the depression to be ejected into the upper layer. This is very similar to the phenomena observed in our experiments. Linden's model is based on the assumptions that the kinetic energy of a vortex ring is converted to an increase in potential energy due to the entrainment through the deflection–recoil process on a timescale that is determined by the density difference and the scale of the vortex ring, and that the area of the depression of the interface, normalized by the size of the ring, changes proportionally to Fr^{-2}. But if one examines figure 5 of Linden (1973) carefully, one finds that the last assumption is true only at smaller Froude numbers and that actually the power index on Fr increases from -2 to 0 as Fr increases. When Linden derived the Fr^3 mixing law from the above assumptions, this observed tendency was neglected. If one is true to the experimental result, one finds rather a Fr^n mixing law where $n' = 3$ only at small Froude numbers and decreases towards 1 as Fr increases. This is almost the same as the variation found in our experiments. It is interesting that Linden's model, when it is modified in a manner that makes it more faithful to his experiment, shows better agreement with our result. Thus the three different kinds of experiments by Turner, Linden and ourself yield essentially the same result that the entrainment rate obeys the Fr^3 law at small Fr numbers and tends to become saturated with an increase in Fr. This suggests that the same transport mechanism is working in the manner assumed by Linden.

5.3. *Application to penetrative convection*

The investigation of the surface mixed layers of the atmosphere and ocean includes the problem of specifying the buoyancy fluxes across the inversion and thermocline. The values of the buoyancy flux are usually reported in the form of B^*/B, where B and B^* denote respectively the buoyancy input from the surface and the buoyancy flux due to entrainment. If the energy released by gravitational instability due to the buoyancy input has completely been used to produce entrainment across the density interface, the ratio B^*/B becomes unity, which is the case assumed by Ball (1960). Evidently this is the theoretically maximum value.

Stull (1976*a*) has summarized the values of this ratio used in models and inferred from observations, showing a wide scatter between zero and unity. Observations of

the atmospheric boundary layer seem to give larger values around 0.1–0.4 (Stull 1976*a*; Caughey & Palmer 1979), whereas laboratory experiments using linearly stratified waters heated from below seem to yield smaller values; 0.11–0.16 by Deardorff *et al.* (1969), 0.12 and 0.19 by Willis & Deardorff (1974) and 0.25 by Deardorff *et al.* (1980). The large values and variation of the ratio obtained from atmospheric observations may be accounted for by simultaneous operation of many processes such as buoyant convection and wind shear. Stull (1976*b*) showed that analysis of field observations that took these processes into account gave a smaller value of $B^*/B = 0.10$. A clear-cut series of observations on convective deepening that was free from wind shear and horizontal motions was reported by Farmer (1975). He observed a developing mixed layer beneath lake ice and obtained the ratio ranging between 0.06 and 0.34 with an average of 0.17. Thus the value of B^*/B around 0.1–0.2 seems plausible. (Deardorff *et al.* (1969), Willis & Deardorff and Farmer gave the ratio R of the negative and positive areas under the buoyancy-flux curve. The values of B^*/B given here were estimated from these ratios using $B^*/B = R^{\frac{1}{2}}$, which is valid for linear profiles of buoyancy flux.)

The corresponding result of our investigation is shown in figure 13, for $B^*/B = F^*/F$. The observed values of F^*/F at the smaller Froude numbers used lie within a range from 0.09 to 0.25, which is in good agreement with the values cited above. Another interesting point is the Froude-number dependence of F^*/F. The theoretical curve indicates that the ratio takes a maximum value of 0.168 at $Fr = 0.46$ and decreases as Fr goes away from this value. The decrease is sharper at larger values of Fr, and when the density difference vanishes the buoyancy flux is reduced to become almost negligibly small.

The Froude-number dependence has been reported by Kantha (1980), who carried out experiments on penetrative convection in a two-layered fluid using salt flux from a porous bed at the top of the water column. The tendency found is somewhat different from ours, however. As Fr increased, his ratio B^*/B increased gradually to around 0.2, and remained at this value for moderate values of Fr. This change as well as the magnitude of B^*/B agrees very well with our result. At larger Froude numbers, however, the value of B^*/B again increased in contrast with our finding. The reason is not clear.

The energy budget within the mixed layer has provided a basic viewpoint in the theoretical treatment of entrainment (Ball 1960; Turner 1973, 1981; Zeman & Tennekes 1977; Sherman *et al.* 1978; Linden 1979, 1980). We here examine the energy budget of our system briefly using the energy ratio R^* introduced by Manins & Turner (1978). This ratio is defined as the ratio of the increase in potential energy due to the redistribution of the initial density profile, to the potential energy made available by buoyancy input from the surface. In the case of stratified two layers separated by a sharp density interface, it can be shown that the energy ratio R^* is exactly equal to the flux ratio B^*/B (see Appendix):

$$R^* = B^*/B. \tag{5.1}$$

Note that this is different from the relation for linear stratifications obtained by Manins & Turner. Figure 13 thus also shows the energy ratio as a function of Fr. It is found that the potential energy supplied by the plume fluid is utilized most efficiently, 16.8%, at $Fr = 0.46$ and less efficiently at both smaller and larger values of Fr. The low efficiency at larger Froude numbers seems to be attributed to energy radiation by internal waves at the interface which became larger as the time of penetration was approached. The low efficiency at smaller values of Fr, on the other

hand, may be due to large shears between the plume fluid and interface, and resulting large energy dissipation, since the depressions of the interface formed by the impingement of a plume are shallow, probably with large shears. This point, however, needs further investigation.

The energy ratio R^* has a similar physical meaning to the flux Richardson number Rf which is defined as the fraction of the available kinetic energy that appears as potential energy produced by mixing. The difference is only that Rf is based on the available kinetic energy, whereas R^* is based on the potential energy made available by buoyancy input. Linden (1979, 1980) has examined many laboratory experiments on mixing in stratified fluids to investigate the behaviour of Rf as a function of the overall Richardson number Ri ($= Fr^{-2}$). He has found that Rf increases from zero as Ri does, reaches a maximum of about 0.13–0.25, and then decreases with further increase in Ri. This is very similar to figure 13. He has examined only the case where the driving force for mixing is mechanical in origin and mixing by convective processes has been excluded. But our experiments are convective in nature. It may thus be considered that the relationship as shown in figure 13 is very general and independent of the nature of the driving force for mixing.

Our experiments thus provide much useful information on the mechanisms of entrainment at the boundary of a mixed layer. There is probably a good similarity between the behaviour of a plume in a confined two-layered region and convective elements in a mixed layer. As pointed out in §2, the motion of the interface produced by the impingement of a plume has much in common with the phenomena revealed by radar observations. There are of course many differences between our experiment and the actual environment. The most serious points would be the use of an isolated source of buoyancy and a quiescent environment and the neglect of interactions among convective elements as pointed out by BT. The use of a continuing plume instead of thermals, which may be better as a model of convective elements in the atmosphere, would not be a serious deficiency, because as far as the entrainment is concerned the behaviour of a plume and thermal are essentially the same, as shown by comparison with Linden (1973).

I wish to thank Professor J. Stewart Turner, F.R.S., for providing good, stimulating surroundings to carry out this investigation. I would also like to thank Ross Wylde-Browne, Derek Corrigan and Joe Micallef for their technical assistance, John Taylor for allowing me to use his apparatus to measure detailed profiles of the vertical density distribution, and Mrs Beryl Palmer for retyping the manuscript several times. Professor Turner read an earlier version of this paper carefully, and his effort is greatly appreciated.

Appendix

Following Manins & Turner (1978), we derive a relation between the energy ratio R^* and flux ratio B^*/B for two stratified layers separated by a sharp density interface. Consider a water column stratified by a salinity difference heated from below. The density profiles are shown in figure 14, where we have assumed a homogeneous buoyancy distribution in the lower mixed layer for the sake of simplicity. This is a good approximation for the asymptotic state. The buoyancy balances for S- and T-profiles are

$$h\beta\,\Delta S = \Delta h\,\beta S_0, \tag{A 1}$$

$$hg\alpha\,\Delta T = -B\,\Delta t, \tag{A 2}$$

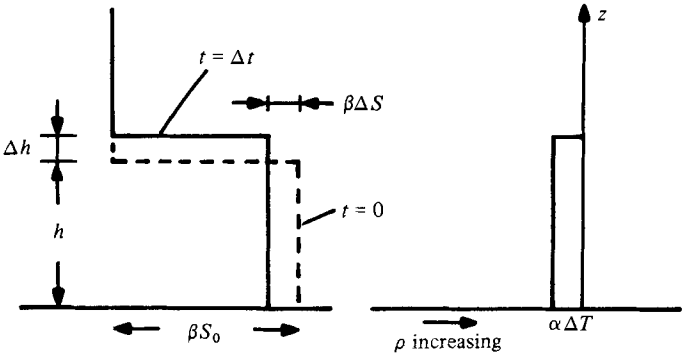

FIGURE 14. The distributions of density due to salinity and heat, produced when the gradient is heated from below.

where g is the acceleration due to gravity, B is the input flux of buoyancy due to heating, and α and β are the coefficients of expansion for T and S respectively ($\alpha < 0$, $\beta > 0$). The buoyancy flux B^* due to entrainment is

$$B^* = g\beta S_0 \frac{\Delta h}{\Delta t}. \tag{A 3}$$

The potential energy released by heating from below, and distributing the heat through the depth h, is given by $E_T = -\frac{1}{2}h^2 g\alpha\,\Delta T$. The increase in the potential energy in the S-field is $E_S = \frac{1}{2}h^2 g\beta\,\Delta S$, where (A 1) has been used. We therefore have

$$R^* = \frac{E_S}{E_T} = -\frac{\beta\,\Delta S}{\alpha\,\Delta T}. \tag{A 4}$$

Substituting for $\beta\,\Delta S$ in (A 4) using (A 1), for $\alpha\,\Delta T$ using (A 2), and using (A 3) results in

$$R^* = B^*/B.$$

REFERENCES

ARNOLD, A. J., ROWLAND, J. R., KONRAD, T. G., RICHTER, J. H., JENSEN, D. R. & NOONKESTER, V. R. 1975 Simultaneous observations of clear air convection by a pulse radar, an FM–CW radar, an acoustic sounder and an instrumented aircraft. *Preprints 16th Radar Meteorology Conf., Houston*, pp. 290–295. AMS.

BAINES, W. D. 1975 Entrainment by a plume or jet at a density interface. *J. Fluid Mech.* **68**, 309–320.

BAINES, W. D. & TURNER, J. S. 1969 Turbulent buoyant convection from a source in a confined region. *J. Fluid Mech.* **37**, 51–80.

BALL, F. K. 1960 Control of inversion height by surface heating. *Q. J. R. Met. Soc.* **86**, 483–494.

CAUGHEY, S. J. & PALMER, S. G. 1979 Some aspects of turbulence structure through the depth of the convective boundary layer. *Q. J. R. Met. Soc.* **105**, 811–827.

DEARDORFF, J. W., WILLIS, G. E. & LILLY, D. K. 1969 Laboratory investigation of non-steady penetrative convection. *J. Fluid Mech.* **35**, 7–31.

DEARDORFF, J. W., WILLIS, G. E. & STOCKTON, B. H. 1980 Laboratory studies of the entrainment zone of a convectively mixed layer. *J. Fluid Mech.* **100**, 41–64.

ELLISON, T. H. & TURNER, J. S. 1959 Turbulent entrainment in stratified flow. *J. Fluid Mech.* **6**, 423–448.

FARMER, D. M. 1975 Penetrative convection in the absence of mean shear. *Q. J. R. Met. Soc.* **101**, 869–891.

GERMELES, A. E. 1975 Forced plumes and mixing of liquids in tanks. *J. Fluid Mech.* **71**, 601–623.

HARDY, K. R. & OTTERSTEN, H. 1969 Radar investigations of convective patterns in the clear atmosphere. *J. Atmos. Sci.* **26**, 666–672.

HOPFINGER, E. J. & TOLY, J. A. 1976 Spatially decaying turbulence and its relation to mixing across density interfaces. *J. Fluid Mech.* **78**, 155–175.

KAIMAL, J. C., WYNGAARD, J. C., HAUGEN, D. A., COTÉ, O. R., IZUMI, Y., CAUGHEY, S. J. & READINGS, C. J. 1976 Turbulence structure in the convective boundary layer. *J. Atmos. Sci.* **33**, 2152–2169.

KANTHA, L. H. 1980 Turbulent entrainment at a buoyancy interface due to convective turbulence. In *Fjord Oceanography* (ed. H. J. Freeland, D. M. Farmer & C. D. Levings), pp. 197–204. Plenum.

KANTHA, L. H., PHILLIPS, O. M. & AZAD, R. S. 1977 On turbulent entrainment at a stable density interface. *J. Fluid Mech.* **79**, 753–768.

KATO, H. & PHILLIPS, O. M. 1969 On the penetration of a turbulent layer into stratified fluid. *J. Fluid Mech.* **37**, 643–655.

KILLWORTH, P. D. & CARMACK, E. C. 1979 A filling-box model of river-dominated lakes. *Limnol. Oceanogr.* **24**, 201–217.

KILLWORTH, P. D. & TURNER, J. S. 1982 Plumes with time-varying buoyancy in a confined region. *Geophys. Astrophys. Fluid Dyn.* **20**, 265–291.

KONRAD, T. G. 1970 The dynamics of the convective process in clean air as seen by radar. *J. Atmos. Sci.* **27**, 1138–1147.

LINDEN, P. F. 1973 The interaction of a vortex ring with a sharp density interface: a model for turbulent entrainment. *J. Fluid Mech.* **60**, 467–480.

LINDEN, P. F. 1979 Mixing in stratified fluids. *Geophys. Astrophys. Fluid Dyn.* **13**, 3–23.

LINDEN, P. F. 1980 Mixing across a density interface produced by grid turbulence. *J. Fluid Mech.* **100**, 691–703.

LOFQUIST, K. 1960 Flow and stress near an interface between stratified liquid. *Phys. Fluids* **3**, 158–175.

MANINS, P. C. 1979 Turbulent buoyant convection from a source in a confined region. *J. Fluid Mech.* **91**, 765–781.

MANINS, R. C. & TURNER, J. S. 1978 The relation between the flux ratio and energy ratio in convectively mixed layers. *Q. J. R. Met. Soc.* **104**, 39–44.

MOORES, W. H., CAUGHEY, S. J., READINGS, C. J., MILFORD, J. R., MANSFIELD, D. A., ABDULA, S., GUYMER, T. H. & JOHNSTON, W. B. 1979 Measurements of boundary layer structure and development over SE England using aircraft and tethered balloon instrumentation. *Q. J. R. Met. Soc.* **105**, 397–421.

MORTON, B. R. 1956 Buoyant plumes in a moist atmosphere. *J. Fluid Mech.* **2**, 127–144.

MORTON, B. R., TAYLOR, G. I. & TURNER, J. S. 1956 Turbulent gravitational convection from maintained and instantaneous sources. *Proc. R. Soc. Lond.* A **234**, 1–23.

SHERMAN, F. S., IMBERGER, J. & CORCOS, G. M. 1978 Turbulence and mixing in stably stratified waters. *Ann. Rev. Fluid Mech.* **10**, 267–288.

SMITH, K. A. & GERMELES, A. E. 1974 LNG tank stratification consequent to filling procedures. *Proc. LNG* 4, *Alger.*

STULL, R. B. 1976*a* The energetics of entrainment across a density interface. *J. Atmos. Sci.* **33**, 1260–1267.

STULL, R. B. 1976*b* Mixed layer depth model based on turbulent energetics. *J. Atmos. Sci.* **33**, 1268–1278.

TURNER, J. S. 1968 The influence of molecular diffusivity on turbulent entrainment across a density interface. *J. Fluid Mech.* **33**, 639–656.

TURNER, J. S. 1973 *Buoyancy Effects in Fluids.* Cambridge University Press.

TURNER, J. S. 1981 Small-scale mixing processes. In *Evolution of Physical Oceanography* (ed. B. A. Warren & C. Wunsch), pp. 236–262. MIT Press.

WARNER, J. & TELFORD, J. W. 1963 Some patterns of convection in the lower atmosphere. *J. Atmos. Sci.* **20**, 313–318.

WARNER, J. & TELFORD, J. W. 1967 Convection below cloud base. *J. Atmos. Sci.* **24**, 374–382.

WILLIS, G. E. & DEARDORFF, J. W. 1974 A laboratory model of the unstable planetary boundary layer. *J. Atmos. Sci.* **31**, 1297–1307.

WOLANSKI, E. J. & BRUSH, L. M. 1975 Turbulent entrainment across stable density step structures. *Tellus* **27**, 259–268.

WORSTER, M. G. & HUPPERT, H. E. 1983 Time-dependent density profiles in a filling box. *J. Fluid Mech.* **132**, 457–466.

ZEMAN, O. & TENNEKES, H. 1977 Parameterization of the turbulent energy budget at the top of the daytime atmospheric boundary layer. *J. Atmos. Sci.* **34**, 111–123.